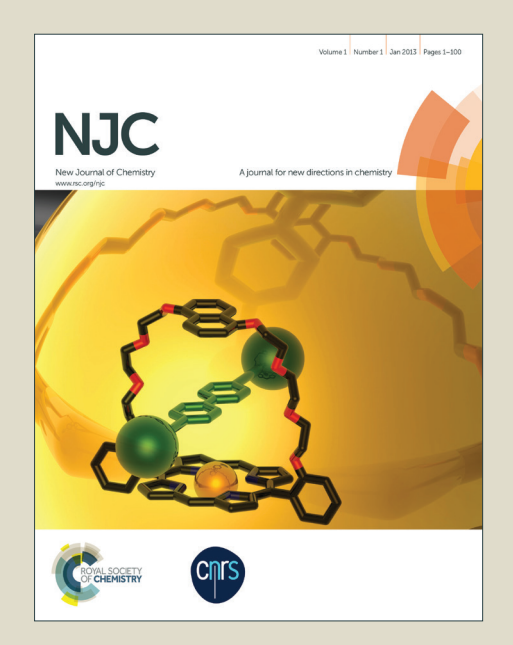
NJC

Accepted Manuscript



This is an *Accepted Manuscript*, which has been through the Royal Society of Chemistry peer review process and has been accepted for publication.

Accepted Manuscripts are published online shortly after acceptance, before technical editing, formatting and proof reading. Using this free service, authors can make their results available to the community, in citable form, before we publish the edited article. We will replace this Accepted Manuscript with the edited and formatted Advance Article as soon as it is available.

You can find more information about *Accepted Manuscripts* in the **Information for Authors**.

Please note that technical editing may introduce minor changes to the text and/or graphics, which may alter content. The journal's standard <u>Terms & Conditions</u> and the <u>Ethical guidelines</u> still apply. In no event shall the Royal Society of Chemistry be held responsible for any errors or omissions in this *Accepted Manuscript* or any consequences arising from the use of any information it contains.



Graphical Abstract

Amino acid mediated functionalization and reduction of graphene oxide - synthesis and formation mechanism of nitrogen-doped graphene

Anil Kumar* and Mahima Khandelwal

Department of Chemistry, Indian Institute of Technology Roorkee, Roorkee - 247667, India Fax: +91 1332 273560; Tel: +91 1332 285799; E-mail: anilkfcy@iitr.ac.in

Amino acid(s) mediated reduction of GO through their nucleophilic attack yield N doped graphene in both acidic and basic media.



Cite this: DOI: 10.1039/c0xx00000x

www.rsc.org/xxxxxx

ARTICLE TYPE

Amino acid mediated functionalization and reduction of graphene oxide - synthesis and formation mechanism of nitrogen-doped graphene

Anil Kumar* and Mahima Khandelwal

Received (in XXX, XXX) Xth XXXXXXXXX 20XX, Accepted Xth XXXXXXXX 20XX 5 DOI: 10.1039/b000000x

This manuscript presents the amino acid(s) mediated functionalization and reduction of graphene oxide (GO) using an environmental friendly method producing N-doped graphene. The reduction of GO by 2-aminoisobutyric acid (AIB) and glycine occurs efficiently in both acidic and mild basic pH conditions. Relatively faster reduction by AIB at pH 10.5 (3 h) compared to that at pH 4.5 (7 h) has been attributed to the increased nucleophilicity of amino and carboxyl groups. Atomic force and electron microscopic studies exhibit the formation of graphene sheets. Selected area electron diffraction analysis and high resolution transmission electron microscopy suggest crystalline nature of these sheets and its in-plane lattice constant was estimated at 0.24 nm. The optical, infrared (IR) and X-ray photoelectron spectroscopy (XPS) indicate the reduction of GO to graphene, whereas, IR, Raman and XPS suggest the functionalization of reduced GO. An increase in I_D/I_G ratio for GRH-AIB (1.02) compared to GO (0.89) suggests an increase in microstructural disorder of reduced GO possibly involving the introduction of some sp³ defects upon functionalization. A mechanism for the functionalization and reduction of GO by amino acids is discussed. Different applications of N- doped graphene are suggested.

1. Introduction

In recent years, graphene has attracted large attention because of its immense scientific and technological potential. It displays unique thermal, mechanical, electronic and optical properties, 20 which have been applied for the fabrication of thermal interface materials,² Nanoelectromechanical system devices,³ thin film transistors, 4 solar cells 5 and fluorescent sensing. 6 Defect free graphene are known to show almost complete optical transparency with high stability, electrical and thermal 25 conductivity, and exceptional mechanical property. 7-9 Such graphene could be beneficial in the areas of electronics, optics, photonics, electromechanical resonators and sensors. 10-13 On the contrary, there have been a number of reports on the transport properties of graphene containing defects as well. The importance 30 of structural defects has been highlighted by Banhart et al. 14 and Jaffri et al. 15 for their utility in designing of devices with improved electronic properties. Defect sites on graphene have also been exploited for sensing of: gases¹⁶ and chemical and biological species.¹⁷ Graphene containing defects has also been 35 used as a metallic wire for making electronic devices. 18 A number of reports have appeared in the literature on the doping of N on the surface of graphene, 19-24 which have been explored for improving their electro-catalytic, electrochemical and storage capabilities. These characteristic features are finding great 40 potential in Li-ion batteries, 20 electrochemical bio-sensing, 21 light emitting diodes, ²² fuel cells, ²³ and ultra-capacitors. ²⁴

A large number of synthesis routes employing different chemical reducing agents such as: hydrazine and its derivatives, 25-28 hydroquinone, 29 sodium borohydride, 30,31 p-45 phenylenediamine, 32 hydrohalic acid, 33 and sulphur containing compounds, 34-35 have been tried for the fabrication of graphene.

In order to minimize their hazardous effect increasing efforts have been put to devise environmental friendly reducing agent(s)/protocols for their synthesis on large scale. Some of the 50 environment friendly reducing agents employed are: reducing sugar, ³⁶ starch-based materials, ³⁷ ascorbic acid, ^{38,39} and certain amino acids. 40,41 Gao et al. have made use of L-ascorbic acid as reductant and L-tryptophan as stabilizer for the reduction of graphite oxide to produce graphene.³⁹ Amino acids and its 55 derivatives have specific advantage because of their non-toxic and biocompatible nature. Recently, two contradictory reports have appeared on the use of glycine as reducing agent for graphene oxide (GO). 41,42 These reports make use of glycine at 10 and 16.6 mM, respectively. In view of this, the present work 60 explores the use of 2-aminoisobutyric acid (AIB), a derivative of glycine along with the glycine (Fig. 1) as reducing agent. It results in the simultaneous reduction and functionalization of reduced GO. It also assisted in probing the mechanism of reduction and functionalization.

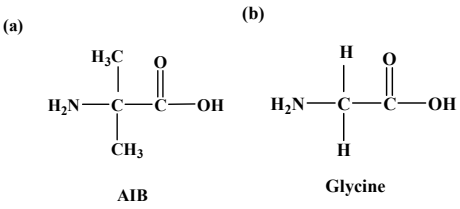


Fig. 1 Structures of: AIB (a) and glycine (b).

2. Experimental

2.1. Materials Used

Natural graphite flakes (75+mesh) and AIB (Aldrich)

hydrochloric acid, hydrogen peroxide (30%), potassium permanganate, phosphorous pentoxide (SD Fine chemicals Ltd.); potassium persulphate (Merck); sulphuric acid (Thomas Baker); glycine and sodium hydroxide pellets (Himedia) were of 5 analytical grades and used without any further purification. Dialysis tubing (seamless cellulose tubing) and dialysis tubing closures were purchased from Sigma. All solutions were prepared freshly in Millipore water.

2.2. Equipment

10 UV-Vis spectra were recorded on a Shimadzu UV2100 spectrophotometer using 1mm quartz cell. Surface topography of the samples was studied by recording 2D images on a NTEGRE (NT-MDT) atomic force microscope (AFM) equipped with NOVA software. Analysis of surface morphologies and elemental 15 analysis were carried out on QUANTA 200-FEG digital field emission scanning electron microscope (FE-SEM) equipped with energy dispersive x-ray analysis (EDAX) facility along with charged-coupled device (CCD) for imaging. Transmission electron micrographs (TEM) and selected area electron 20 diffraction (SAED) measurements were recorded on a FEI-TECNAI G² 30 and G² 20 at an accelerating voltage of 300 and 200 kV, respectively for different magnifications. X-ray diffraction pattern of powder samples were recorded on a Bruker AXS D8 Advance X-ray diffractometer (XRD) using Cu Kα line 25 (1.5418 Å) of the X-ray source at 40 kV and 30 mA. The diffraction patterns were recorded in 20 range of 50 to 400 at a scan rate of 0.01⁰ per step. Infrared (IR) spectra were recorded on a Thermo Nicolet Nexus Fourier transform infrared (FTIR) spectrophotometer equipped with OMNIC v6.1 software in mid 30 IR range (4000 - 400 cm⁻¹) in KBr medium. Raman measurements were carried out on an inVia Renishaw spectrophotometer serial no. 021R88 and H33197 equipped with confocal microscope using Ar ion 514 nm laser excitation having 1 cm⁻¹ spectral resolution in Raman shift and confocal resolution 35 of 2.5 µm. X-ray photoelectron spectroscopy (XPS) measurements were performed on an Omicron nanotechnology instrument using Al Ka energy source (1486.6eV). Thermogravimetric analysis (TGA) was carried out on a SII TG/DTA 6300 EXSTAR instrument in the temperature range of 40 25°C-700 °C in N₂ atmosphere, at a heating rate of 10 °C/min.

2.3. Methodology

Samples for TEM analysis were prepared by applying a drop of the dilute sample on a carbon coated copper grid G-200 (size 3.05 mm). The excess sample from the grid was removed with the help 45 of a tissue paper. This grid was dried in dark at room temperature for about 30 min to evaporate the remaining moisture prior to its analysis. Electron micrographs of these samples were recorded by scanning the dried grid at different magnifications under the electron microscope at an accelerating voltage of 300/200 kV. 50 ImageJ software was used for analyzing TEM images, specifically for calculating the d spacing in high resolution transmission electron microscopy (HRTEM) images. Samples for FE-SEM and AFM analysis were prepared by applying a drop of dilute sample on the glass substrate which was dried at room 55 temperature in the dark. The FE-SEM images were recorded by applying an acceleration voltage of 20 kV. AFM images were recorded in a semi-contact mode. For AFM experiments, the

scanning frequency was varied in the range of 1.5 to 3.13 Hz and data were recorded at room temperature. Height measurements 60 along the line of the AFM image were carried out by using NOVA software. XRD, XPS and FTIR measurements of solid samples were obtained by drying the sample in vacuum oven at 50 °C for 6 h.

2.4. Synthesis of GO

65 GO was synthesized from natural graphite flakes by a modified Hummers method. 43,44 Graphite flakes (1.5 g) were added into the solution containing the mixture of concentrated H₂SO₄ (6 mL), $K_2S_2O_8$ (1.25 g) and P_2O_5 (1.25 g) preheated at 80 °C. The resulting mixture was stirred at this temperature for 4.5 h using 70 oil bath, cooled to room temperature and then diluted with deionised water (DIW) and, thereafter, left overnight. Subsequently, it was filtered and washed with DIW using a 2-20 micron filter to remove the residual acid. The product was dried under ambient conditions overnight in vacuum desiccator. The 75 pre-treated graphite flakes were then put into ice cold (0 °C) concentrated H₂SO₄ (60 mL). KMnO₄ (7.5 g) was added to this solution gradually under stirring by maintaining the temperature below 20 °C. Thereafter, the resulting mixture was stirred at 35 ^oC for 2 h on oil bath, followed by the addition of 125 mL DIW. 80 The addition of water was carried out in an ice bath to keep the temperature < 50 $^{\circ}$ C. The mixture was further stirred for 2 h at 35 ⁰C, and then additional 350 mL of DIW and 10 mL of 30% H₂O₂ were added sequentially into the mixture. The color of mixture changed from greenish black to brilliant yellow. This mixture was 85 left undisturbed for 24 h. The resulting mixture was centrifuged and washed with 10% aqueous HCl (1 L) followed by 1 L of DIW to remove any remaining acid. The product was dried at 50 ⁰C for 24 h and diluted to make a GO dispersion (5 mg/ml). GO dispersion was then dialysed for one week to remove the 90 remaining any metal species.

GO (0.5 mg/ml) dispersion was exfoliated into DIW by sonication under ambient condition for 30 min. The GO dispersion was left undisturbed overnight to settle down the remaining unexfoliated GO which was a negligible fraction of the 95 total content. The resulting homogeneous yellow brown dispersion was stable for several months and used for reduction.

2.5. Functionalization and Reduction of GO using AIB

In the present protocol for functionalization and chemical reduction of GO to graphene sheets, 52 mg of AIB (25 mM) was 100 mixed with 20 ml of GO dispersion (0.5 mg/ml) under stirring and the pH of the resulting solution was maintained at 4.5 and increased to 10.5 by adding dilute NaOH. This reaction was performed using water bath as well as heating plate equipped with stirrer and temperature sensor. The completion of the 105 reaction on water bath takes about 3 h at 95 °C, whereas on heating plate it required only 1 h at 100 °C. The completion of the reaction was adjudged by noting a change in the color of the reaction mixture, which changed gradually from yellow-brown to homogenous black. The resultant black solid was centrifuged and 110 washed with DIW from five to six times to remove any residual AIB as it is soluble in water. The product obtained was redispersed in DIW maintaining the pH(s) of the solution as mentioned above. The product(s) obtained at high and low pH has been denoted by GRH-AIB and GRL-AIB, respectively. The

amounts of AIB and GO and the time of heating of the reaction mixture were optimized by varying the amount of AIB:GO by monitoring the product. The maximum amount of GRH-AIB/GRL-AIB corresponded to AIB:GO ratio and time of - 5.2:1 5 and 3 h; 5.2:1 and 7 h, respectively. Thereafter, any increase in the ratio did not affect the efficiency and time of reduction. It suggests that the optimum concentration of the reductant plays an important role in accomplishing of reduction. As regards to the previous reports on reducing capabilities of glycine, 41,42 a 10 difference in concentration of glycine might have resulted in different observations from two laboratories.

In control experiments, the functionalization and reduction of GO was also performed using glycine as a reducing agent maintaining the reaction mixture at high and low pH of 10.5 and 15 4.5 under identical conditions and have been denoted as GRH-Gly and GRL-Gly, respectively.

3. Results

3.1. Optical studies

The absorption spectrum of GO displays a peak at 230 nm and a 20 shoulder at 302 nm, which can be attributed to $\pi - \pi^*$ transition due to C=C and n- π * transition corresponding to the C=O group (Fig. 2A-a (Inset)). In the presence of AIB at pH 10.5, a regular change in color from yellowish brown to black takes place. The black color product thus obtained was then suspended into water 25 at pH 10.5, which depicted an optical absorption at 263 nm (Fig. 2A-b). This red shift has been attributed to the increase in the electron density and structural reorganisation in GO suggesting its reduction into graphene. In order to explore the mechanism of the reduction process, this reaction was also carried out at a pH 30 4.5. The absorption spectra of the product obtained at this pH

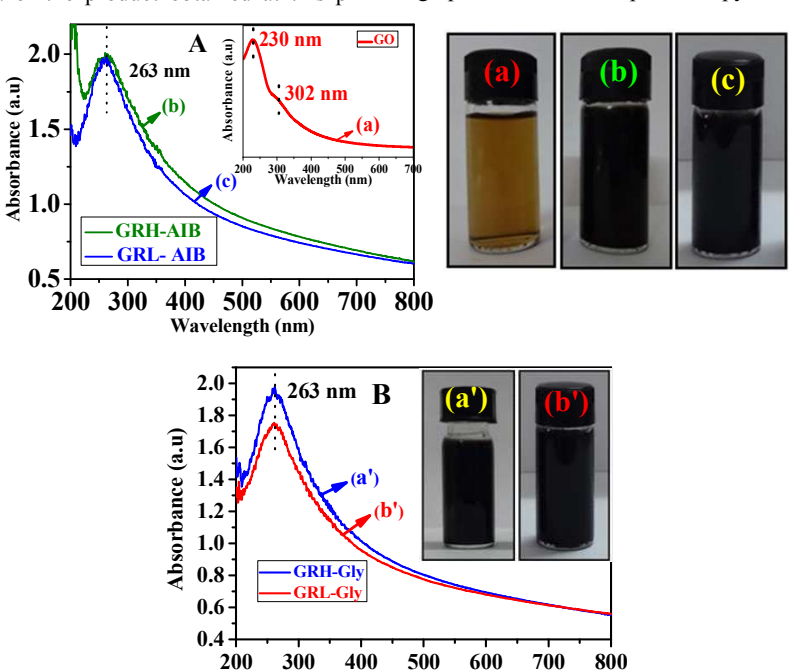
shows the optical absorption very similar to that obtained at pH 10.5 (Fig. 2A-c). At pH 4.5, the amino group of AIB is expected largely to be protonated. Under these conditions the complete reduction of GO took about 7 h, which is about 2.3 times longer 35 to that of at pH 10.5. Digital photographs of GO, GRH-AIB and GRL-AIB obtained by dispersing them in water at their respective pH are shown in the adjacent diagram to Fig. 2A. The dark black color for GRH-AIB and GRL-AIB compared to that of GO is quite apparent from this diagram.

In order to examine the reducing capability of glycine, the reduction of GO was performed under similar conditions to those used for AIB. The complete reduction of GO by glycine at pH of 10.5 and 4.5 takes about 3 and 10 h, respectively. The absorption spectra of the product(s) obtained at these pHs and their 45 respective digital photographs are shown in Fig. 2B. These results clearly reveal that similar to that of AIB, glycine is equally effective for the reduction of GO at both the pHs.

In a control experiment the reduction of GO was also performed by using NaOH as reductant at pH 10.5. The complete 50 reduction of GO into graphene using NaOH (Fig. S1, ESI†) took more than 13 h, which is enormously longer as compared to those of GRH-AIB and GRH-Gly, which gets completed in ≤ 3 h. It is even longer to those of GRL-AIB and GRL-Gly, which are completed in 7 and 10 h, respectively. Within 3 h, we could not 55 find any significant conversion of GO to graphene by OH at pH 10.5 which was confirmed by recording its optical absorption (Fig. S2, ESI†). The observations that AIB and glycine are able to reduce GO at high as well as low pH effectively, it clearly indicates them to be quite effective as reductants.

60 3.2. Raman analysis

In order to work out the electronic structure of the as synthesised graphene, Raman spectroscopy was used to analyze the



65 Fig. 2 Optical absorption spectra of: GO (a) - (Inset), GRH-AIB (b) and GRL-AIB (c) - (Panel A) along with their digital photographs captured by dispersing them in water given in adjacent Fig.: GO (a), GRH-AIB (b) and GRL-AIB (c). Optical absorption spectra of GRH-Gly (a') and GRL-Gly (b'); Inset - Digital photographs of: GRH-Gly (a') and GRL-Gly (b') - (Panel B).

Wavelength (nm)

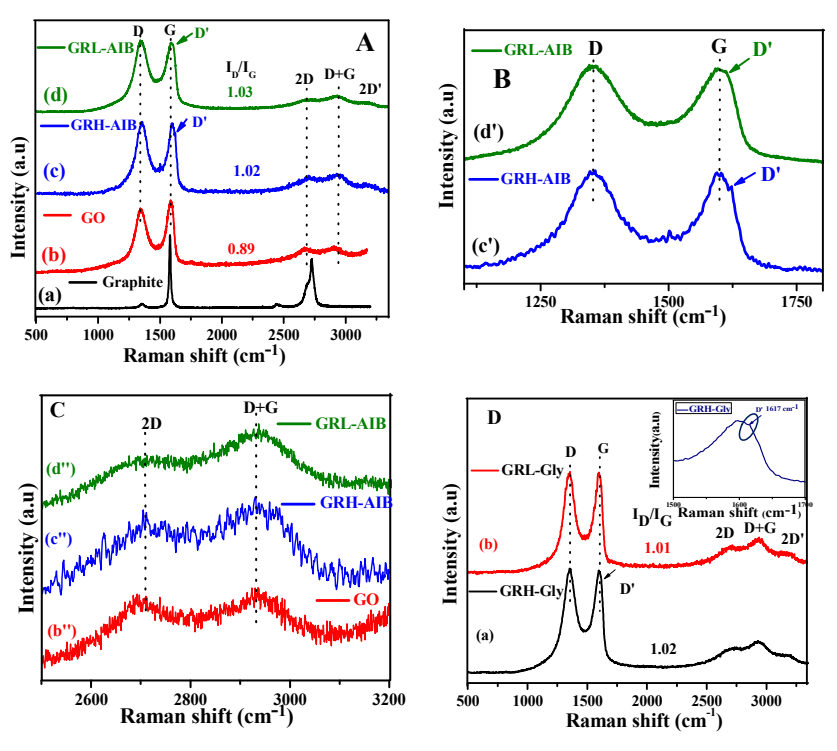
precursors (graphite and GO) along with the reduction product of GO using AIB as reductant at pH 10.5 (GRH-AIB). These spectra are shown in (Fig. 3) and the corresponding spectral data are 5 summarized in Table S1 in ESI†. The Raman spectrum of graphite shows characteristic D, G, 2D₁ and 2D₂ bands (cm⁻¹) at 1357 (small), 1575 (sharp), 2687 (shoulder) and 2727 (sharp), respectively (Fig. 3A-a) as assigned earlier.⁴⁵ The sample of GO exhibits four peaks at 1357, 1601, 2699, 2934 cm⁻¹ (Fig. 3A-b) 10 matching fairly well to previous reports on GO⁴⁶ and have been assigned to its D, G, 2D and D+G bands, respectively. A comparison of Raman spectrum of GO with graphite shows that the shape of the peak due to D and G bands are fairly different and broad in case of GO. Moreover, 2D band is shifted to higher 15 frequency, besides an additional band appears at 2934 cm⁻¹. It possibly arises by mixing of D and G bands. In this case the ratio of I_D/I_G was evaluated to be 0.89.

The Raman spectrum due to GRH-AIB depicted six bands (cm 1) at: 1351, 1598, 1623 (shoulder), 2709, 2932 and 3194, which 20 have been assigned as D, G, D', 2D, D+G and 2D' bands (Fig. 3A-c), respectively. The frequencies of these bands are fairly different compared to that of GO. A close examination of these frequencies reveals that the intensity of D band at 1351 cm⁻¹ is increased and G band is shifted to lower energy by 3 cm⁻¹ and a 25 new shoulder is developed at 1623 cm⁻¹ (D' band) (Fig. 3B-c'). All these features suggest that the reduced GO may be N-doped in the present case similar to that noted earlier in previous report. 47 The peaks observed at 2709 and 3194 cm⁻¹ (not shown) are assigned as the second order peak due to D and G bands, 30 respectively and the peak at 2932 cm⁻¹ could be attributed to the

D+G combination band (Fig. 3C-c"). An examination of 2D band compared to that of graphite shows a blue shift by 18 cm⁻¹. Such a blue shift is indicative of doped graphene similar to that observed in earlier report. 48 The increase in ratio of I_D/I_G (1.02) 35 for GRH-AIB compared to GO (0.89) suggests an increase in disorder in microstructures of reduced GO. It might also involve the introduction of some sp³ defects upon functionalization.⁴⁹ This aspect was further used to calculate the in-plane crystallite size (L_a) of the doped graphene, from which the value of L_a was 40 worked out to be 16.5 nm. This value is fairly small compared to that of GO (18.9 nm) suggesting that the reduction/doping leads to a decrease in crystallite size.

Raman spectrum of GRL-AIB is shown in Fig. 3A-d. It exhibits all the features as regards to the different Raman bands 45 very similar to that of observed in GRH-AIB. An analysis of this spectrum also showed the characteristic D' band (Fig. 3B-d') and a similar I_D/I_G ratio of 1.03. It clearly indicates that the nature of the product at this pH is also the same as obtained at pH 10.5.

The reduction of GO by glycine was also analyzed by 50 recording their Raman spectrum at pH 10.5 and 4.5 and are shown in Fig. 3D. Features of Raman spectra for GRH-Gly and GRL-Gly are recorded in Fig. 3D-a and b and for these samples the ratio of I_D/I_G was found to be 1.02 and 1.01, respectively. A comparison of these spectra with those obtained for GRH-AIB/ 55 GRL-AIB (Fig. 3A-c and d) shows them to be very similar indicating the glycine also to be equally effective reducing agent for GO. Hence, further studies on its characterization have been performed for GRH-AIB sample only.



60 Fig. 3 Raman spectra of: Graphite (a), GO (b), GRH-AIB (c) and GRL-AIB (d) - (Panel A); Expanded Raman spectra of: GRH-AIB (c') and GRL-AIB (d') in 1100-1800 cm⁻¹ range (Panel B). Expanded Raman spectra of: GO (b"), GRH-AIB (c") and GRL-AIB (d") in 2500-3200 cm⁻¹ range (Panel C). Raman spectra of: GRH-Gly (a), (Inset) - Expanded D' and GRL-Gly (b) - (Panel D).

3.3. XRD analysis

The XRD patterns of graphite, GO and GRH-AIB are shown in Fig. 4. The graphite flakes depicts the characteristic sharp and intense peak at 26.3° corresponding to the plane (002) with a d s spacing value equal to 0.338 nm. The GO obtained by the oxidation of graphite shows (002) reflection at much lower angle at 10.4° with a fairly high d spacing value at 0.85 nm which has been assigned to the intercalation of water molecule and oxygen containing functional groups between the layers of the graphite. 10 XRD pattern due to GRH-AIB was fairly different to both of its precursors and exhibit a broad (002) reflection at 23.1° with a d spacing of 0.385 nm.

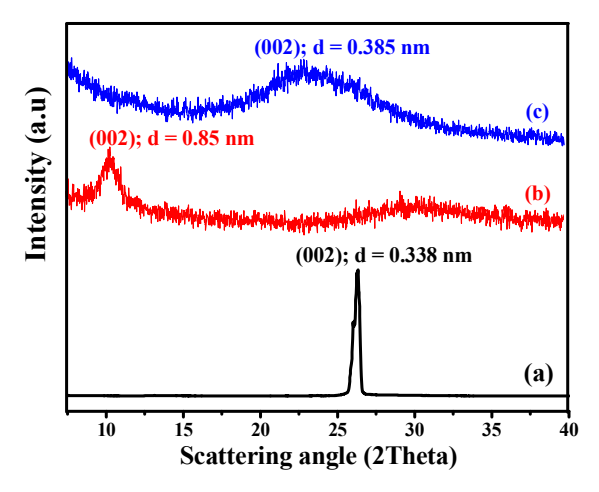


Fig. 4 XRD patterns of: Graphite (a), GO (b) and GRH-AIB (c).

15 3.4. AFM measurements

AFM images of GO and GRH-AIB are shown in Fig. 5 a and b. respectively. It exhibits the formation of sheet like structure in both the cases. Using NOVA software, the thickness of these sheets was examined along a line at various locations and shown 20 at a particular location in Fig. 5 a' and b', respectively. From the height profile, the average height for these samples along a line was measured to be 1.25 and 0.83 nm, respectively. The observed variation in height suggest the GO and GRH-AIB sheet to be 1-2 layers thick.³⁸ Relatively smaller average height of GRH-AIB 25 compared to GO might have resulted due to the removal of

oxygenated groups from the surface of GO.

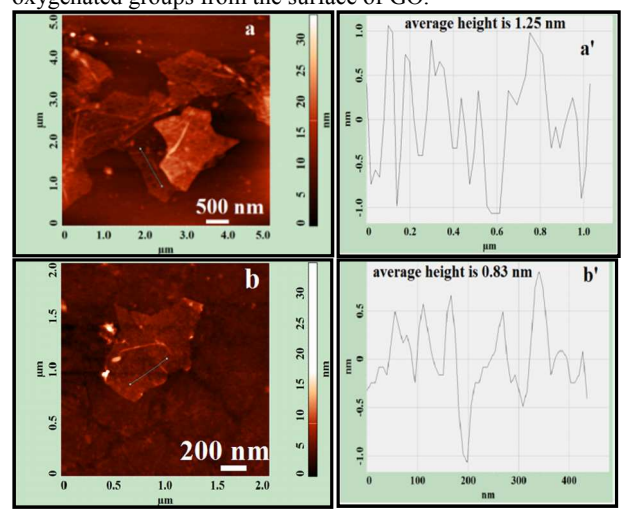


Fig. 5 AFM images and their height profile along a line: GO (a,a') and 30 GRH-AIB (b,b'), respectively.

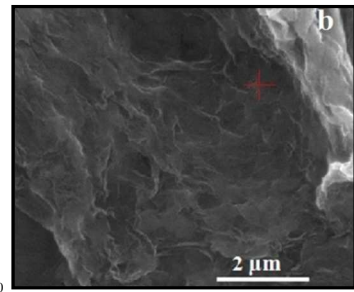
3.5. FE-SEM and EDAX analysis

FE-SEM images of GO and GRH-AIB are shown in Fig. 6 a and b and their EDAX analysis on a particular location marked by cross sign in red are shown in the adjacent Tables and the 35 corresponding EDAX spectrum are shown in Fig. S3 in ESI†. The FE-SEM image(s) of GO shows it to be layered structure having the dimension of about $25 \times 20 \mu m$ (Fig. S4A ESI†). The FE-SEM image due to GRH-AIB consists of folded transparent sheets (Fig. 6b). The dimension of this sheet was recorded from 40 its other image recorded at low resolution (Fig. S4B ESI†), and was estimated to be about 20 × 20 μm. In contrast to GRH-AIB, the image due to GO appeared to have the rough surface.

An analysis of elemental composition of GO and GRH-AIB has been compiled in Table S2 in ESI†. As expected GRH-AIB 45 shows to be rich in carbon content having C to O ratio of 8.4:1 which is about more than 4 times higher to that of GO (2.0:1) (Table S2). It also contains 3.23 at.% N. The contribution of Si in this analysis has arisen from the used glass substrate.

	Y.	7	a
	1		
1		P	5 μm

Element	Wt%	At%
CK	43.70	56.65
OK	28.97	28.20
SiK	27.33	15.15
Matrix	Correction	ZA



V	Element	Wt%	At%
Я	CK	72.51	81.09
Ŋ	NK	03.36	03.23
S	OK	11.48	09.64
1	SiK	12.64	06.05
P	Matrix	Correction	ZAF
6			

Fig. 6 FE-SEM images and their EDAX analysis on a particular location marked by cross sign in red are shown in the adjacent Tables: GO (a) and GRH-AIB (b), respectively.

3.6. TEM and SAED analysis

- 55 The TEM and HRTEM images of GO exhibits a sheet like structure (Fig. 7 a and a'). The HRTEM image of this sheet shows some fringes on its edges. An analysis of these fringes gives estimated interplanar distance of 0.80 ± 0.05 nm corresponding to (002) plane, which is higher to that of graphite (0.338 nm). Its 60 SAED pattern in the inset of Fig. 7a shows concentric rings
- masked with bright spots indicating it to be of polycrystalline nature. TEM image of GRH-AIB (Fig. 7b) also indicates it to consist of wrinkled nanosheets. The wrinkles at various places suggest it to contain only a few layers of graphene as was also
- 65 indicated by the low density of materials at these locations. SAED analysis of the GRH-AIB also clearly exhibits the nature of graphene sheets to be crystalline with six fold symmetry (Inset

- Fig. 7b). The HRTEM image of GRH-AIB (Fig. 7b') exhibits fringes all along the sheet. The fringes were observed at different resolutions and a typical image at highest resolution is shown in Fig. 7b'. From the analysis of this image the value of lattice 5 constant was found to be 0.24 nm, which corresponds to the in plane lattice constant 'a'. From the HRTEM image recorded at another magnification an interlayer spacing was estimated at 0.38 nm (Fig. S5A in ESI†). It may be noted that the measured dspacing of 0.38 nm is higher than that of graphite (0.338 nm). It 10 has possibly arisen because of an increase in microstructural disorder of graphene by the incorporation of nitrogen. The functionalization by N introduces some sp³ defects as was evidenced by Raman analysis. Such an increase in d- spacing has also been reported earlier for the synthesis of graphene using 15 hydrazine as reducing agent. 50 The corresponding 2D Fast Fourier Transform (FFT) image shows the hexagonal pattern (Fig. S5B in ESI†), it thus clearly confirms the presence of hexagonal sp² carbon features.

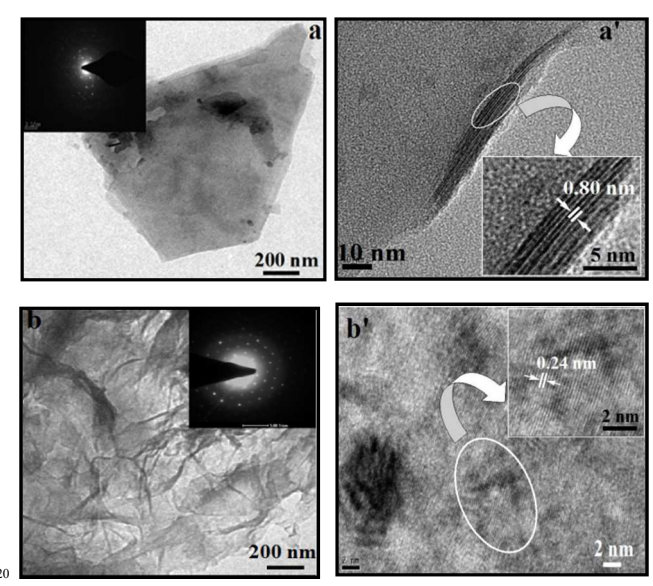
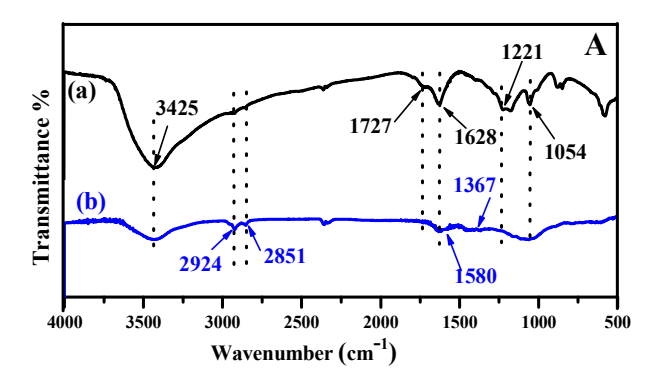


Fig. 7 TEM and HRTEM images of: GO (a,a'), and GRH-AIB (b,b'), (inset) - SAED pattern, respectively.

3.7. IR studies

Fig. 8 (a and b) in panel A presents the FTIR spectra of GO and 25 GRH-AIB. The precursor, GO exhibits various prominent bands (cm⁻¹) at: 3425, 1727, 1628, 1221, 1054 which have been assigned to: OH, C=O present in COOH, C=C, C-O-C (epoxy) and C-O (alkoxy) groups, respectively. In the IR spectrum of GRH-AIB the peak due to free OH is significantly reduced and 30 new bands appeared at 2924 and 2851 cm⁻¹ due to symmetric and asymmetric stretching of the C-H, respectively. IR spectra of GO and GRH-AIB on the expanded scale between 1800-1300 cm⁻¹ are presented in Fig. 8 (a' and b') in panel B. A comparison of the IR spectra of GO with GRH-AIB depicts a significant change in 35 the vibrational bands, besides several new weak and broad peaks are also developed for the latter sample. The peak due to C=O at 1727 cm⁻¹ vanished completely in GRH-AIB. However, the peak at 1628 cm⁻¹ due to the C=C bonds still exists in GO and GRH-AIB. Whereas, in the case of GRH-AIB new peaks with poor 40 absorption have appeared in the frequency range (cm⁻¹) from: 1580 – 1542 and 1367, which may be assigned to N-H bending

and C-N stretching, respectively. Similar observations were earlier made by Lee et al. in the case of glycine as a reducing agent. 41 However, none of these bands were reported for the 45 reduction of graphite oxide using L-ascorbic acid as reductant and L- tryptophan as stabilizer.³⁹ The peak due to alkoxy group (C-O) at 1054 cm⁻¹ in graphene also became fairly weak and broad. A comparison of the IR spectra of GRH-AIB and GO shows that the peak due to epoxy (1221 cm⁻¹) in GO has fully 50 disappeared suggesting its complete reduction.



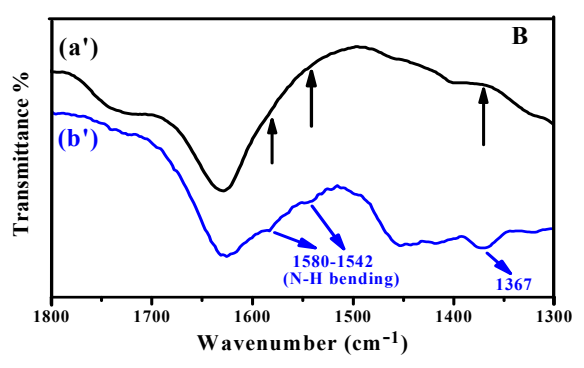


Fig. 8 FTIR spectra of: GO (a) and GRH-AIB (b) - (Panel A); Expanded FTIR spectra of: GO (a') and GRH-AIB (b') in 1800-1300 cm⁻¹ range 55 (Panel B).

3.8. XPS analysis

In order to further analyze the surface of as synthesised GRH-AIB, its XPS spectrum was recorded in 0-800 eV range (Fig. 9). XPS spectra of GO and GRH-AIB in the entire scan energy range 60 are shown in Panel A. Panel B shows the C 1s spectrum of GO which depicts the four peaks at (eV): 284.2, 286, 286.7 and 287.9 which can be assigned to the sp² carbon corresponding to C=C, C-OH, C-O of epoxy/alkoxy and C=O of carboxylic groups, respectively. Similarly, C 1s spectrum of GRH-AIB containing 65 different bands at 284.4, 285.6, 286.4, 288.1 eV can be assigned to C=C, C-N corresponding to N-sp²C, C-O of epoxy/alkoxy and C=O of carboxylic groups, respectively (Panel C). A comparison of C 1s spectra due to GO and GRH-AIB reveals that in case of GRH-AIB the peak due to C=C corresponding to sp² carbon is 70 enhanced whereas peak due to C=O and C-O corresponding to carboxylic and epoxy/alkoxy are reduced and C-OH peak is completely vanished. In addition a new peak owing to C-N corresponding to N-sp²C is developed. These changes are understood due to an increase in graphitic character in GRH-AIB 75 and doping of N, respectively. To further examine the nitrogen configuration in graphene, N 1s spectrum (Panel D) was

deconvoluted to various peaks in different energy range, which can be assigned to pyridinic N at 398.1 eV, pyrolic N at 399.3 eV and quaternary N at 400.3 eV, respectively. O 1s peak due to GO and GRH-AIB are shown in Panel E at 531.7 and 532 (eV), 5 respectively. A decrease in intensity of O 1s peak in GRH-AIB along with a high energy shift indicates that the component due to C-O corresponding to epoxy is decreased. The formations of different N configurations in graphene have been indicated in the Scheme given in Panel F. The observation about doping of N in 10 the present system is similar to that reported by Lee et al. 41 who employed glycine as reducing agent and is different to that of Gao et al.³⁹ who made use of L-ascorbic acid as reducing agent and L-tryptophan as stabilizer.

3.9. TGA analysis

15 The thermal stability of graphite, as synthesized GO and GRH-AIB were examined by recording TGA from ambient temperature

to 700 °C and are shown in Fig. 10. The TGA of graphite shows behaviour very similar to that observed in earlier literature.³⁶ The TGA curve due to GO exhibits a mass loss of about 15% at 20 around 100 °C and 43% at around 235 °C and has been assigned to the removal of adsorbed water and labile oxygen containing functional groups CO, CO2 respectively. The second process starts at about 450 °C and a major loss in this process occurs up to 600 °C corresponds to about 87%. Whereas, the TGA curve due 25 to GRH-AIB under similar conditions shows only 10% loss up to 100 °C and 18% loss up to 235 °C. The third major loss of weight starts around 450 °C and at 600 °C it comes out to be about 72%. Moreover, this behaviour is very similar to that observed in a previous study on N doped graphene.⁵¹ After 650 ⁰C virtually 30 there was no further loss, which suggests relatively higher stability of GRH-AIB compared to GO.

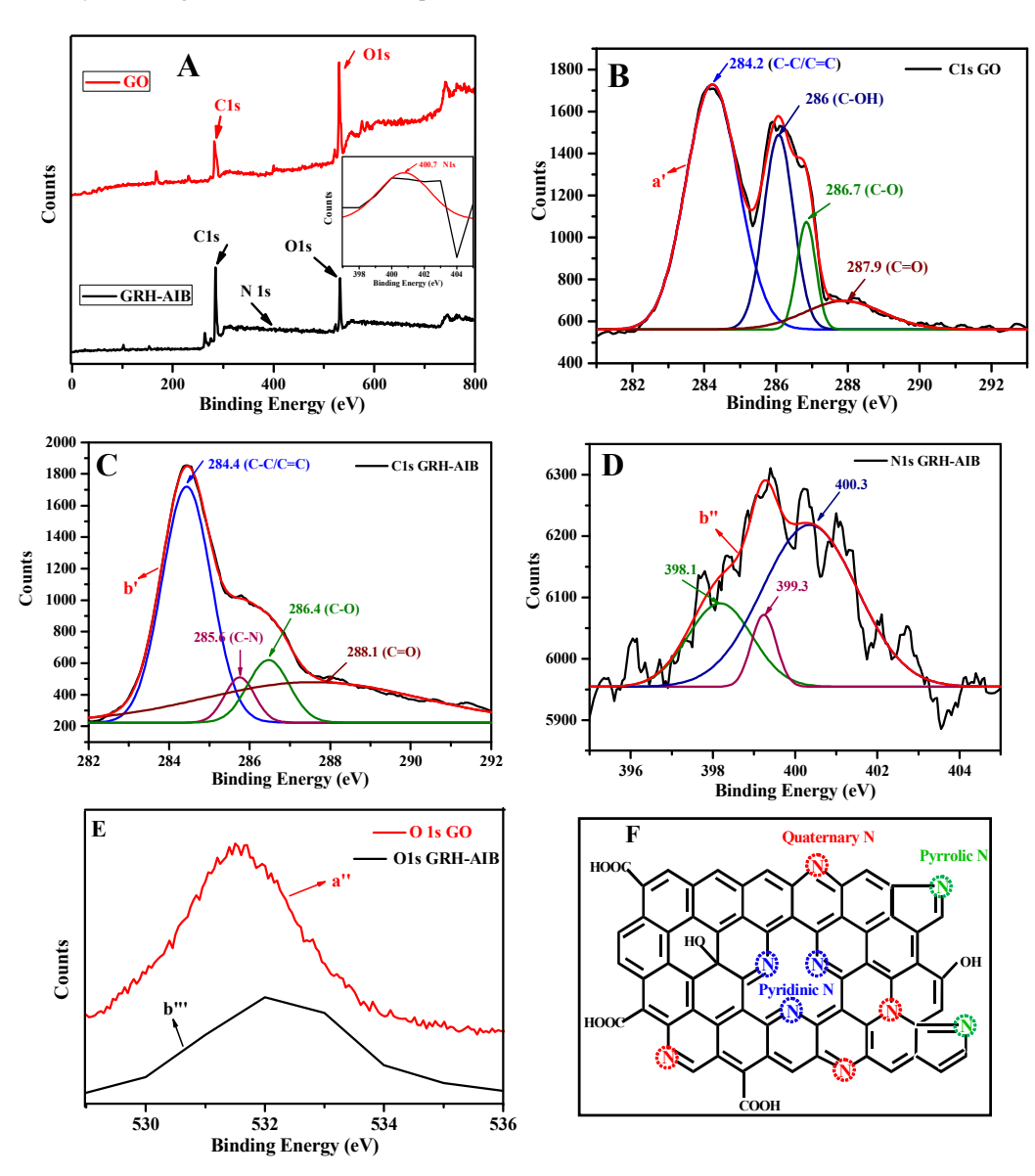


Fig. 9 XPS spectra of: GO (a) and GRH-AIB (b), Inset N 1s - (Panel A); GO C1s (a') - (Panel B); GRH-AIB C1s (b') - (Panel C); GRH-AIB N 1s (b") -(Panel D); GO O 1s (a") and GRH-AIB O 1s (b"') – (Panel E); Schematic presentation of N-doped graphene – (Panel F).

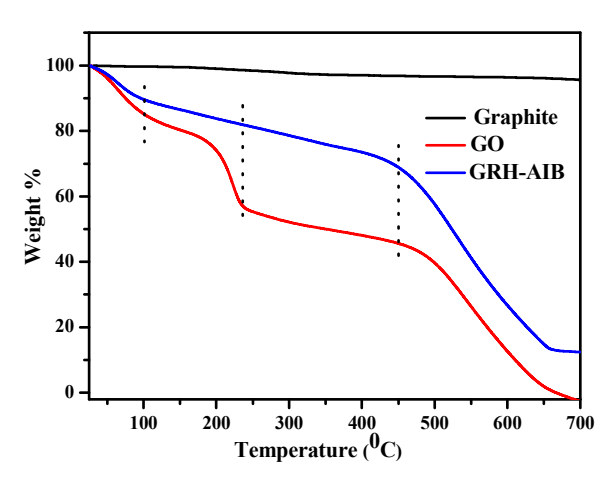


Fig. 10 TGA curves of: Graphite (black), GO (purple), and GRH-AIB (red).

5 **4.** Discussion

The reduction of GO both by AIB and glycine at high (10.5) as well as low (4.5) pH clearly indicates the efficient reduction of GO to graphene, as was evidenced by the observed changes in the optical absorption in the two cases (Fig. 2). These observations 10 are also very well supported by Raman spectroscopic measurements made at high and low pH, respectively (Fig. 3) and are understood in terms of the ratio of I_D/I_G. For the typical case of AIB, the value of I_D/I_G at high (1.02) and low (1.03) pHs were very similar and fairly higher to that of GO (0.89) suggesting an 15 increase in disorder in microstructures of reduced GO. The fact that the time taken for the reduction of GO at low pH was slightly higher compared to that at high pH, (Section 2.5) it suggests the involvement of basic -NH2 and -COO groups in the reduction at high pH, whereas at low pH since -NH₂ group will be largely 20 protonated it reduces the efficiency of reduction. Comparisons of the efficiency of reduction of GO by AIB and glycine at low pH show the later to be relatively less efficient, as was revealed by longer time taken by glycine (10 h) as compared to AIB (7 h). This is also understood by the difference in the structure of these 25 substrates (Fig. 1).

The effect of pH can be appreciated in terms of the pK_a(s) of these substrates. AIB and glycine has two p $K_a(s)$ of: 2.36 (p K_1) and 10.21 (pK₂); 2.34 (pK₁) and 9.6 (pK₂), respectively. Both AIB as well as glycine exhibit very similar reduction efficiency at 30 high pH. At pH of 10.5, it is estimated that about 66% of AIB will be in the basic form, it is likely that the basic AIB act as nucleophile through -NH2 and -COO groups and attacks the epoxy/ hydroxyl group of GO to form an intermediate X, which upon the loss of water at 95°C / 100°C yield graphene along with 35 other decarboxylation products (Scheme 1 and Scheme S1, ESI†). However, from the pK₂ of glycine it is estimated that at pH 10.5 glycine will be more basic (89%) and could act more effectively as nucleophile through -NH₂ compared to AIB. But the similar efficiency in the two cases can be understood by a difference in 40 their electronic structure (Fig. 1). The +I effect of methyl groups in AIB results in the increased electron density at -NH₂ group, which may be contributing to the observed difference. It also explains the same duration of reduction in cases of AIB and

glycine at high pH despite of the higher percentage of basic 45 glycine. On the other hand the pK₁ being similar for the two, at low pH, where reduction prominently takes place by nucleophilic attack through COO (Scheme S1, ESI†), more time taken by glycine as compared to AIB might have arisen due to the electronic effect of two methyl groups in AIB. At low pH it is 50 likely that protonated amino group (-NH₃⁺) interacts with GO involving cationic-pi interaction (Scheme S2 in ESI†) as has been earlier reported by J. Wang et al. 52

The formation of acetone and formaldehyde in cases of AIB /glycine along with graphene (Scheme 1) were confirmed by 55 performing their chemical analysis. Acetone formation was analyzed by preparing its 2,4- dinitrophenyl hydrazone⁵³ and the formation of formaldehyde was tested by its characteristic spot test with chromotropic acid.⁵⁴ Their formation in the present systems was verified with their respective authentic sample.

Since the used amino acids in acidic medium at pH 4.5 itself act as better reductant as compared to OH-, it clearly rules out the participation of OH in affecting the reduction of GO. It also points out the involvement of -NH₂ and COO groups in bringing the reduction of GO at high pH and mainly -COOH at low pH. 65 This finding is in line with the earlier observation of Lee et al. 41 in which they observed glycine to be effective reducing agent for GO.

Scheme 1 Mechanism showing the nucleophilic attack of -NH₂ group of 70 AIB on the epoxy group of GO and resulting in the formation of N-doped graphene.

An analysis of GRH-AIB by XRD (Fig. 4) clearly shows the formation of graphene, which was also evidenced by SAED and HRTEM analysis (Fig. 7). The formation of folded transparent 5 sheets for GRH-AIB is quite apparent by AFM, FESEM and TEM images (Figs. 5-7). From AFM study, the average thickness of sheet was found to be slightly less for GRH-AIB as compared to that of GO. The observed height profiles of GO and GRH-AIB sheets by AFM at different locations suggests them to be about 1-10 2 layers thick (Fig. 5). GRH-AIB has a high ratio of C/O (8.4:1) compared to that of GO (2.0:1), suggesting the GRH-AIB to have more sp² character (Fig. 6). The presence of hexagonal sp² carbon features is also revealed by SAED analysis and FFT image (Figs. 7b- Inset and S5B, ESI†).

An interaction through -NH₂ group is indicated by IR analysis in which, weak peaks due to C-N stretching and N-H bending were observed at 1376 and 1580 – 1542 cm⁻¹, respectively, suggesting the possibility of N doping. The reduction of GO was associated with a significant reduction in the intensity of peaks 20 due to C=O of carboxylic and C-O of epoxy groups. The doping of N is also indicated by Raman spectroscopy in which a new band (shoulder) is developed at 1623 cm⁻¹ (D' band), which is associated by an increase in the ratio I_D/I_G. Earlier also such a behavior has been interpreted due to doping of N. 47 It is further 25 confirmed by XPS analysis which exhibited the development of new peak due to C-N bond. Based on the deconvolution of N 1s spectrum, presence of different N configurations in graphene could be assigned to: pyridinic N at 398.1 eV, pyrolic N at 399.3 eV and quaternary N at 400.3 eV, respectively Fig. 9 (Panel F).

30 **5.** Conclusions

The present manuscript reports an efficient and environmental friendly method for the preparation of graphene employing hydrothermal approach in both acidic (4.5) as well as basic (10.5) pH range using AIB and glycine as functionalizer and reducing 35 agents. The reduction of GO has been monitored by UV-visible, IR, Raman spectroscopy and estimation of C/O ratio by EDAX analysis. For AIB at a pH of 10.5, it takes less than half the time (3 h) to that of in the acidic medium (7 h), which are significantly shorter as compared to previous reports on similar system (~ 24 40 h). 41 It produces a few layer thick crystalline graphene sheets having six-fold symmetry. Functionalization of reduced GO by AIB introduces N in graphene. An increase in the I_D/I_G ratio for GRH-AIB compared to that of GO suggests an increase in defects in the reduced GO, possibly involving the introduction of some 45 sp³ defects upon functionalization in sp² graphitic structure. N doping possibly takes place through nucleophilic attack of -NH₂ and -COO groups of AIB on the epoxy/ hydroxyl group(s) of GO via the formation of an intermediate to yield graphene along with other decarboxylation products. N- doped graphene are 50 finding tremendous applications for the development of Li-ion batteries, field-effect transistors, electrocatalyst for fuel cells, and ultra-capacitors.⁵⁵ Thus we have successfully synthesized Ndoped graphene sheet by employing amino acid(s) as a reducing agent and water as a solvent.

55 Acknowledgements

M.K. is thankful to MHRD, New Delhi for the award of SRF. Thanks are also due to Heads, IIC, IITR, Roorkee for providing the facility of TEM, FE-SEM and AFM, respectively. Authors also acknowledge the help of Prof. B. Viswanathan, IIT Madras,

60 Chennai for XPS; Mr Rahul Bhardwaj and USIC, Delhi University, Delhi for TEM and Raman and M/s Renishaw for Raman facilities, respectively.

Notes

Department of Chemistry, Indian Institute of Technology Roorkee, 65 Roorkee - 247667, India

Fax: +91 1332 273560; Tel: +91 1332 285799; E-mail: anilkfcy@iitr.ac.in; akmshfcy@gmail.com

†Electronic Supplementary Information (ESI) available: Optical absorption of GRH-OH after 13 and 3 h of reaction; EDAX 70 analysis of FESEM images of GO and GRH-AIB; FE-SEM images of GO and GRH-AIB recorded at lower resolutions; HRTEM and FFT image of GRH-AIB; I_D/I_G ratio of various samples; Scheme S1 depicting the mechanism of nucleophilic attack of carboxylic group of AIB on the epoxy group of GO and 75 Scheme S2 showing the Cationic-Pi interaction of protonated amino group of AIB with GO, respectively; tables of spectral data of Raman and FE-SEM. See DOI: 10.1039/b000000x/

References

80

- 1 J. Yao, Y. Sun, M. Yang and Y. Duan, J. Mater. Chem., 2012, 22, 14313.
- 2 K. M. F. Shahil and A. A. Balandin, Solid State Commun., 2012, 152. 1331.
- J. T. Robinson, M. Zalalutdinov, J. W. Baldwin, E. S. Snow, Z. Wei, P. Sheehan and B. H. Houston, Nano Lett., 2008, 8, 3441.
- K. S. Novoselov, A. K. Geim, S. V. Morozov, D. Jiang, Y. Zhang, S. V. Dubonos, I. V. Grigorieva and A. A. Firsov, Science, 2004, 306, 666.
 - M. He, J. Jung, F. Qiu, Z. Lin, J. Mater. Chem., 2012, 22, 24254.
 - M. Liu, H. Zhao, S. Chen, H. Yu, Y. Zhang and X. Quan, Biosens. Bioelectron., 2011, 26, 4213.
- G. Eda, G. Fanchini, M. Chhowalla, Nat. Nanotech., 2008, 3, 270.
- X. Wang, L. Zhi and K. Müllen, *Nano Lett.*, 2008, 8, 323,
- U. Khan, K. Young, A. O'Neill and J. N. Coleman, J. Mater. Chem., 2012, 22, 12907.
- 10 S. Gilje, S. Han, M. Wang, K. L. Wang and R. B. Kaner, Nano Lett., 2007, 7, 3394.
- 11 F. Bonaccorso, Z. Sun, T. Hasan and A. C. Ferrari, Nat. Photon.,
- 12 J. S. Bunch, A. M. Van der Zande, S. S. Verbridge, I. W. Frank, D. M. Tanenbaum, J. M. Parpia, H. G. Craighead and P. L. McEuen, Science, 2007, 315, 490.
 - 13 F. Schedin, A. K. Geim, S.V. Morozov, E.W. Hill, P. Blake, M. I. Katsnelson and K. S. Novoselov, Nat. Mater., 2007, 6, 652.
 - 14 F. Banhart, J. Kotakoski and A. V. Krasheninnikov, ACS Nano, 2010, 5, 26.
 - 15 S. H. M. Jafri, K. Carva, E. Widenkvist, T. Blom, B. Sanyal, J. Fransson, O. Eriksson, U. Jansson, H. Grennberg, O. Karis, R. A. Quinlan, B. C. Holloway and K. Leifer, J. Phys. D: Appl. Phys. 2010, 43, 045404.
- 16 Q. Huang, D. Zeng, S. Tian and C. Xie, Mater. Lett., 2012, 83, 76. 110
 - 17 Y. Shao, J. Wang, H. Wu, J. Liu, I. A. Aksay and Y. Lin, Electroanalysis, 2010, 22, 1027.
 - 18 J. Lahiri, Y. Lin, P. Bozkurt, II. Oleynik and M. Batzill, Nat. Nanotech., 2010, 5, 326.
- 19 Z. Mou, X. Chen, Y. Du, X. Wang, P. Yang and S. Wang, Appl. Surf. Sci., 2011, 258, 1704.
 - 20 A. L. M. Reddy, A. Srivastava, S.R. Gowda, H. Gullapalli, M. Dubey and P. M. Ajayan, ACS Nano, 2010, 4, 6337.

- 21 Y. Wang, Y. Shao, D. W. Matson, J. Li and Y. Lin, ACS Nano, 2010, 4, 1790.
- 22 J. O. Hwang, J. S. Park, D. S. Choi, J. Y. Kim, S. H. Lee, K. E. Lee, Y-H. Kim, M. H. Song, S. Yoo and S. O. Kim, ACS Nano, 2012, 6,
- 23 L. Qu, Y. Liu, J-B. Baek and L. Dai, ACS Nano, 2010, 4, 1321.
- 24 H. M. Jeong, J. W. Lee, W. H. Shin, Y. J. Choi, H. J. Shin, J. K. Kang and J. W. Choi, Nano Lett., 2011, 11, 2472.
- 25 S. Stankovich, R. D. Piner, X. Chen, N. Wu, S. T. Nguyen and R. S. Ruoff, J. Mater. Chem., 2006, 16, 155
- 26 S. Stankovich, D.A. Dikin, R. D. Piner, K. M. Kohlhaas, A. Kleinhammes, Y. Jia, Y. Wu, S. T. Nguyen and R. S. Ruoff, Carbon, 2007, 45, 1558.
- V. C. Tung, M. J. Allen, Y. Yang and R. B. Kaner, Nat. Nanotech., 2009, 4, 25-29.
- 28 S. Stankovich, D. A. Dikin, G. H. B. Dommett, K. M. Kohlhaas, E. J. Zimney, E. A. Stach, R. D. Piner, S. T. Nguyen and R. S. Ruoff, Nature, 2006, 442, 282.
- 29 G. Wang, J. Yang, J. Park, X. Gou, B. Wang, H. Liu and J. Yao, J. Phys. Chem. C, 2008, 112, 8192.
- 30 W. Gao, L. B. Alemany, L. Ci and P. M. Ajayan, Nat. Chem., 2009,
- 31 H-J. Shin, K. K. Kim, A. Benayad, S-M. Yoon, H. K. Park, I-S. Jung, M. H. Jin, H-K. Jeong, H. M. Kim, J-Y. Choi and Y. H. Lee, Adv. Funct. Mater., 2009, 19, 1987.
- 32 Y. Chen, X. Zhang, P. Yu and Y. Ma, Chem. Comm., 2009, 30, 4527.
- 33 S. Pei, J. Zhao, J. Du, W. Ren and H. M. Cheng, Carbon, 2010, 48,
- 34 W. Chen, L. Yan and P. R. Bangal, J. Phys. Chem. C, 2010, 114, 19885
 - 35 T. Zhou, F. Chen, K. Liu, H. Deng, Q. Zhang, J. Feng and Q. Fu, Nanotechnology, 2011, 22, 045704.
 - 36 C. Zhu, S. Guo, Y. Fang and S. Dong, ACS Nano, 2010, 4, 2429.
- Y. Feng, N. Feng and G. Du, RSC Adv., 2013, 3, 21466.
 - 38 J. Zhang, H. Yang, G. Shen, P. Cheng, J. Zhang and S. Guo, Chem. Comm., 2010, 46, 1112.

- 39 J. Gao, F. Liu, Y. Liu, N. Ma, Z. Wang and X. Zhang, Chem. Mater., 2010, 22, 2213.
- 40 D. Chen, L. Li and L. Guo, Nanotechnology, 2011, 22, 325601.
 - S. Bose, T. Kuila, A. K. Mishra, N. H. Kim and J. H. Lee, J. Mater. Chem., 2012, 22, 9696.
- M. J. Fernández-Merino, S. Villar-Rodil, J. I. Pardes, P.; Guardia, L. Solís-Fernández, R. García, A. Martínez-Alonso and J. M. D. Tascón, Carbon, 2013, 63, 30.
- W. S. Hummers and R. E. Offeman, J. Am. Chem. Soc., 1958, 80,
- 44 Y. Xu, H. Bai, G. Lu, C. Li and G. Shi, J. Am. Chem. Soc., 2008, 130, 5856.
- 50 45 A. C. Ferrari, J. C. Meyer, V. Scardaci, C. Casiraghi, M. Lazzeri, F. Mauri, S. Piscanec, D. Jiang, K.S. Novoselov, S. Roth and A. K. Geim, Phys. Rev. Lett., 2006, 97, 187401.
 - 46 K. Liu, J-J. Zhang, F-F. Cheng, T-T. Zheng, C. Wang and J-J. Zhu, J. Mater. Chem., 2011, 21, 12034.
- 55 47 H. Liu, Y. Zhang, R. Li, X. Sun, S. Désilets, H. Abou-Rachid, M. Jaidann and L-S. Lussier, Carbon, 2010, 48, 1498.
 - 48 C. He, Z. Li, M. Cai, M. Cai, J-Q. Wang and Z. Tian, J. Mater. Chem. A, 2013, 1, 1401.
- 49 V. Georgakilas, M. Otyepka, A.B. Bourlinos, V. Chandra, N. Kim, K.C. Kemp, P. Hobza, R. Zboril and K.S. Kim, Chem. Rev., 2012, 112, 6156.
 - 50 G. Srinivas, Y. Zhu, R. Piner, N. Skipper, M. Ellerby and R. Ruoff, Carbon, 2010, 48, 630.
- 51 Z. Lin, M-K. Song, Y. Ding, Y. Liu, M. Liu and C-P. Wong, Phys. Chem. Chem. Phys., 2012, 14, 3381.
- 52 J. Wang, Y. Zhao, F-X. Ma, K. Wang, F-B. Wang and X-H. Xia, J. Mater. Chem. B, 2013, 1, 1406.
- 53 O. L. Brady and G.V. Elsmie, Analyst, 1926, 51, 77.
- 54 J. Mitchell, I. M. Kolthoff, E. S. Prosakauer and A. Weissberger, Organic Analysis, Interscience Publishers, New York, 1961.
 - 55 H. Wang, T. Maiyalagan and X. Wang, ACS Catalysis, 2012, 2, 781.